Flagellated Janus particles for multimodal actuation and transport

(iD) **Louis William Rogowski,** (iD) **Xiao Zhang,** (iD) **Jiannan Tang,** (iD) **Micah Oxner,** (iD) **Min Jun Kim, et al.**

COLLECTIONS

(F) This paper was selected as Featured

(SCI) This paper was selected as Scilight

View Online   Export Citation   CrossMark

ARTICLES YOU MAY BE INTERESTED IN

Flagellated Janus particles for multimodal actuation and transport (F) (SCI)

Louis William Rogowski, (iD) Xiao Zhang, (iD) Jiannan Tang, (iD) Micah Oxner, (iD) and Min Jun Kim[a] (iD)

AFFILIATIONS

Department of Mechanical Engineering, Southern Methodist University, Dallas, Texas 75205, USA

[a]**Author to whom correspondence should be addressed:** mjkim@lyle.smu.edu

ABSTRACT

Catalytic Janus particles rely on chemical decomposition to self-propel and have displayed enormous potential for targeted drug delivery and cellular penetration. Catalytic propulsion mechanisms are limiting, however, with fuel requirements and specialized fluid properties being necessary to achieve propulsion. We have improved the dynamic propulsion of catalytic Janus particles by functionalizing flagellar filaments to one of their hemispheres. Flagellated Janus particles, torqued by rotating magnetic fields, swim along their rotation axis using the explicit chirality and flexibility of flagella, mimicking flagellar rotation of live bacteria. Depending on the working fluid, flagellated Janus particles can propel using either catalytic or swimming propulsion. We demonstrate experimentally that flagellated Janus particles behave predictably under the two actuation modes and can precisely follow trajectories under closed-loop feedback control. Flagellated Janus particles were demonstrated to swim in both Newtonian and shear-thickening fluids. These are the first Janus particles developed that can be propelled interchangeably between catalytic and flagellar swimming propulsion, allowing two distinct propulsion mechanisms for future use within *in vivo* operations.

Published under an exclusive license by AIP Publishing. https://doi.org/10.1063/5.0053647

INTRODUCTION

Janus particles are typically composed of two materially different hemispheres,[1,2] allowing for diverse physical interactions and responses to stimuli from the surrounding fluid.[3] For these reasons, Janus particles have displayed surprising versatility as enhanced minimally invasive drug delivery platforms,[4,5] made strides toward manipulating the processes of biological organisms,[6] and have successfully navigated in *in vivo* environments.[7] Methods for propelling Janus particles include light actuation,[8] attachment to live bacteria,[9] enzyme enabled catalysis,[10] hydrophobic–hydrophilic interactions,[11] and multi-fueled catalyzation.[12,13] Most Janus particles rely on chemical catalyzation[3,14] to propel within viscous force dominated low Reynolds number environments, where specific chemical concentrations are needed to guarantee propulsion.[15] Multiple catalysts exist in the literature with one of the most common being platinum (Pt), which is used to greatly accelerate the naturally occurring decomposition reaction of hydrogen peroxide (H$_2$O$_2$),

$$2H_2O_2 \xrightarrow{Pt} 2H_2O + O_2. \tag{1}$$
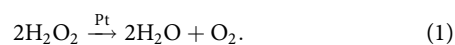
The propulsive force generated from H$_2$O$_2$ decomposition is sufficient to propel Janus particles through bulk fluids and at boundaries.[14,16–19] Catalytic Janus particles were found to have their propulsion velocities inversely proportional with their diameter[20] and proportional to the concentration of H$_2$O$_2$ in the surrounding fluid.[21] Likewise, the structure of the platinum surface coating and the physical geometries of the Janus particles were also found to play a role in influencing propulsion direction during catalysis.[22,23] While H$_2$O$_2$ is toxic in high concentrations (>9%), the effects from short term exposure can be alleviated using intravenous medicine.[24–26] Even so, chemical actuation by itself is not always viable for *in vivo* operation, particularly in regions of the body that possess viscosities much higher than water,[19,27] such as in the gastrointestinal tract.[28] In such high viscosity regions, it would be beneficial to have access to another motion mode that is reliable, can be activated remotely without the presence of specific chemical agents, and can be used without fear of chemical toxicity.

Rotating magnetic fields are a common actuation method for many microrobotic platforms since they are biocompatible and have long-range transmissibility. Many microswimmers have been

designed in the literature to effectively couple rotation and translation from a magnetic field using symmetry considerations; examples of these include achiral magnetic particles,[29] flagellated nanoswimmers,[30–32] helical microswimmers,[33] and soft microrobots.[34] Microscale swimming requires that microrobots either have a chiral geometry (such as a helix) or some flexibility in order to produce time irreversible strokes in low Reynolds number environments;[15] this prevents perfectly symmetric microparticles (including Janus particles) from propelling in Newtonian fluids under pure rotation. While symmetric microparticles have been demonstrated to propel by spontaneous symmetry breaking within some nonlinearly viscoelastic fluids,[35] this propulsion is not always available, and alternatively, a more explicit mechanism of symmetry breaking is required to propel Janus particles under rotating fields.

Presented here are catalytic Janus particles that were chemically functionalized with bacterial flagella harvested from *Salmonella typhimurium* (SJW 1103). The attached flagella explicitly break the apparent symmetry of the spherical Janus particles since they are both flexible and chiral in shape, allowing for mobility matrices that can efficiently convert applied rotational torques into linear translation;[36,37] as the microparticle rotates, it acts as a large motor that rotates the attached flagella, mimicking live bacteria. These multimodal microrobots, dubbed flagellated Janus particles (FJPs), can be propelled using either catalytic propulsion from H_2O_2 or through swimming propulsion induced by rotating magnetic fields. Janus particles that were physically attached to live bacteria have been explored previously;[38] however, researchers did not directly control the bacteria's motion and instead relied on the random run and tumble of the bacteria to distribute the Janus particles. Similarly, hybrid systems developed using a combination of sperm and artificial magnetic microstructures were shown to be guided by magnetic fields for drug delivery, but relied entirely on live sperm as the sole propulsion mechanism.[39] Here, externally applied static and rotating magnetic fields can be used to directly change the velocity and direction of FJPs under swimming propulsion, while catalytic propulsion can be directionally navigated using purely static magnetic fields. FJPs were fabricated using streptavidin coated ferromagnetic microparticles that were coated with platinum on one hemisphere, using e-beam evaporation,[40] while the other hemisphere was functionalized with flagella using an avidin–biotin chemical reaction (see Materials and Methods).[37] Figure 1(a) presents a generalized schematic of the FJPs, while Fig. 1(b) shows a compressed *z*-stacked image of an actual FJP observed using an Olympus confocal laser scanning microscope (FV3000) with a 60× objective, where several flagella are attached along its right surface. The distribution of flagella was found to vary heavily between Janus particles due to the stochastic nature of this self-assembly and the non-uniform avidin surface coating that remained after Janus particle fabrication (see Materials and Methods). Despite this stochastic assembly, propulsion was ubiquitous and easy to achieve for FJPs under both motion modes. This is the first time Janus particles possessing both catalytic and flagella-based swimming propulsion mechanisms have been developed. The FJPs presented here were directly controlled using externally applied magnetic fields from an approximate Helmholtz coil system. Subsequent sections will demonstrate both the reliable velocity responses and directional control under both motion modes in both Newtonian and

non-Newtonian fluids. A full description of the magnetic field controller and the FJP fabrication process can be found in Materials and Methods.

RESULTS

Comparative velocity performance

After fabrication, both swimming and catalytic propulsion modes of FJPs were investigated separately to quantify their behavior. The FJPs were first suspended inside a de-ionized water solution, containing 5% H_2O_2 and 5% Tween 20 by concentration, to examine their velocity under catalysis; the Tween 20 was added to prevent FJPs from sticking to the substrate surfaces of the sample chamber and reduce contact friction. Catalytic propulsion was limited to surface motion throughout these experiments due to gravity driven sedimentation from the weight of the particles. The 5% concentration of H_2O_2 was chosen in order to reduce the rate of bubbles formed within the sample chamber [see Eq. (1)] and allowed for prolonged experimentation (~20 min) before serious microscopy visualization issues occurred. Once a catalytically propelling FJP was located, it was tracked using image processing (see Materials and Methods), and its instantaneous velocity was calculated. Using the magnetic field controller (see Materials and Methods), the FJPs were directed to follow along a user-determined trajectory within the *x*–*y* plane [Figs. 1(c) and 1(d)]. Due to heterogeneous differences during fabrication, an offset between the magnetic dipoles and the platinum coating created a randomized propulsion offset angle Ψ relative to the static field direction [Fig. 1(d)]. This offset angle did not noticeably affect the propulsive capabilities of the FJPs during experiments. The results of this analysis produced graphs like the one seen in Fig. 2(a), which shows the moving average velocity (30-point window) over a 52 s time interval for six different FJPs; each FJP had at minimum three independent trials. While each FJP had slight variations in its velocity as time progressed due to changes in contact surface friction, the velocity profiles were relatively constant overall. For the six different FJPs examined under catalytic propulsion, with each of them having at least three independent trials each, Fig. 2(b) shows a bar graph displaying their average velocity and standard deviation over a 30 s time period; the average velocity, μ, and the standard deviation, σ, for each observed FJP can be seen in Table I. The average velocity tended to vary between different FJPs, either because of friction along the substrate or differences in the platinum coatings, but they all maintained stable velocities between multiple trials and were able to propel for prolonged periods of time. While the velocities achieved by the FJPs under catalytic propulsion were relatively slow, these velocities can be improved by increasing the H_2O_2 concentration in the surrounding fluid as was shown in the previous literature.[21]

Another batch of FJPs was next suspended inside of a 15%–30% NaCl solution, without H_2O_2 present in the medium, in order to test the efficiency of their swimming propulsion. The 15%–30% NaCl gave the Janus particles a neutral buoyancy and allowed them to remain far from the boundaries of the sample chamber ($\geq 100\,\mu$m), where all experiments regarding swimming propulsion occurred. The same approximate Helmholtz coil system was used to generate rotating magnetic fields to actuate the FJPs in
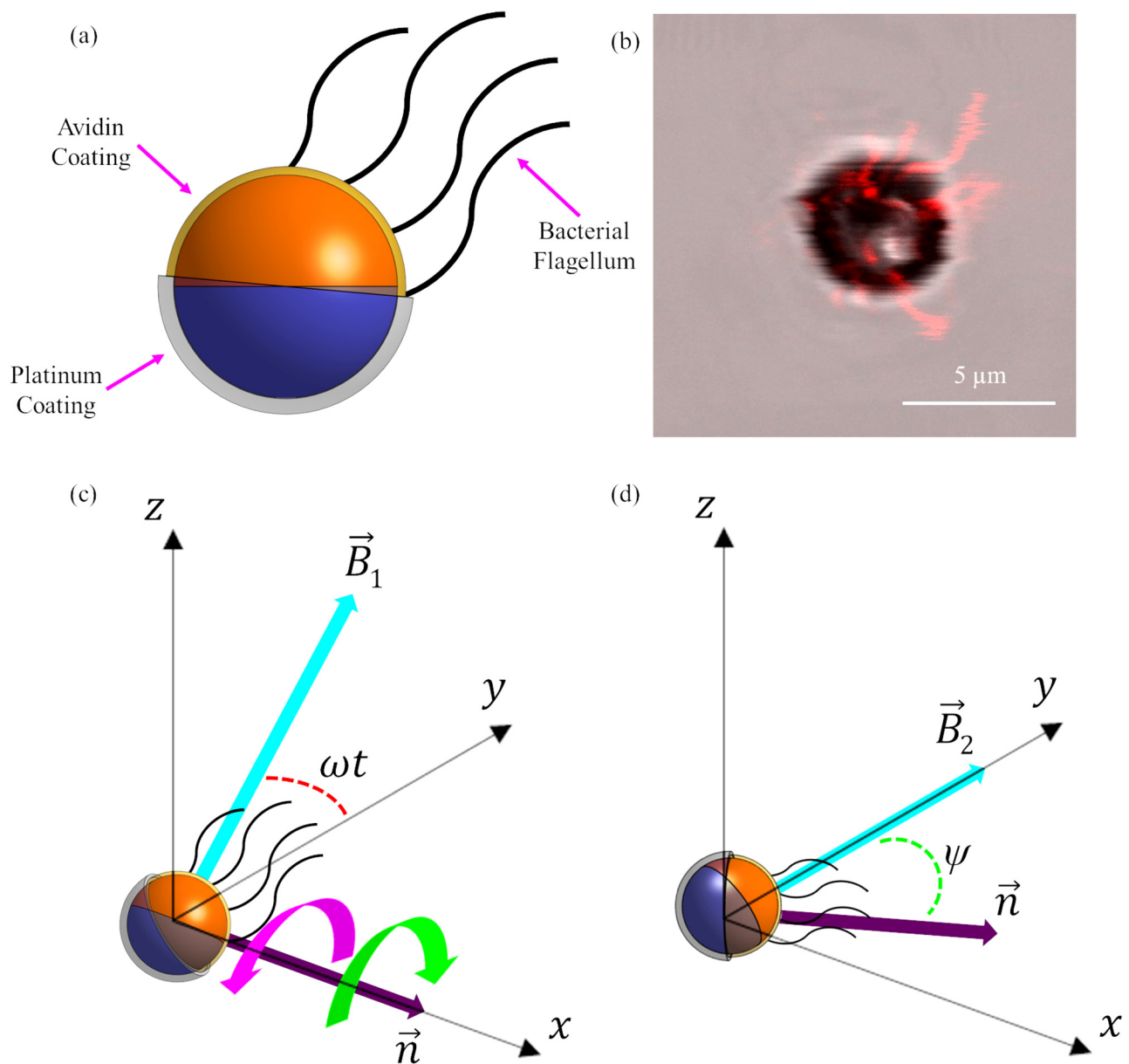
FIG. 1. Morphology of flagellated Janus particles. (a) Schematic of the flagellated Janus particle. Platinum coating enables catalytic propulsion, while the flagella allow for swimming propulsion. Blue and orange hemispheres represent the magnetic dipoles of the Janus particle. (b) Flagellated Janus particle with flagella distributed along its surface. Flagella are attached through an avidin–biotin chemical functionalization. Flagella were visualized using an Olympus confocal microscope (FV3000) with a 60× objective with a Cy3 excitation laser. (c) Janus particle actuated using rotational magnetic fields, where $\vec{B_1}$ rotates the dipoles around the direction vector $\vec{n}$; attached flagellum will enable swimming motion along $\vec{n}$. When viewed from behind $\vec{n}$, the magnetic field can rotate either counterclockwise or clockwise depending on the sign of the frequency. (d) Janus particle actuated using chemical catalyzation. The magnetic field, $\vec{B_2}$, orients the dipoles of the Janus particle, while the chemically induced propulsion propels the particle along $\vec{n}$ at offset angle Ψ, which is the offset of the platinum coating from the magnetic dipoles. The heading angles θ were set to 0° and 90° for (c) and (d), respectively. See Materials and Methods for a full description of magnetic field controllers for each motion mode.

conjunction with a superimposed static field (see Materials and Methods). To understand velocity as a function of rotating magnetic field frequency f, the superimposed static field was fixed at a constant value during each experiment, while the rotating magnetic field was increased proportionally with frequency in order to prevent step out ($B_r = 0.175f$, see Materials and Methods);[41] the frequency range selected for these experiments was between 5 and 50 Hz. Only the velocity along the intended propulsion direction
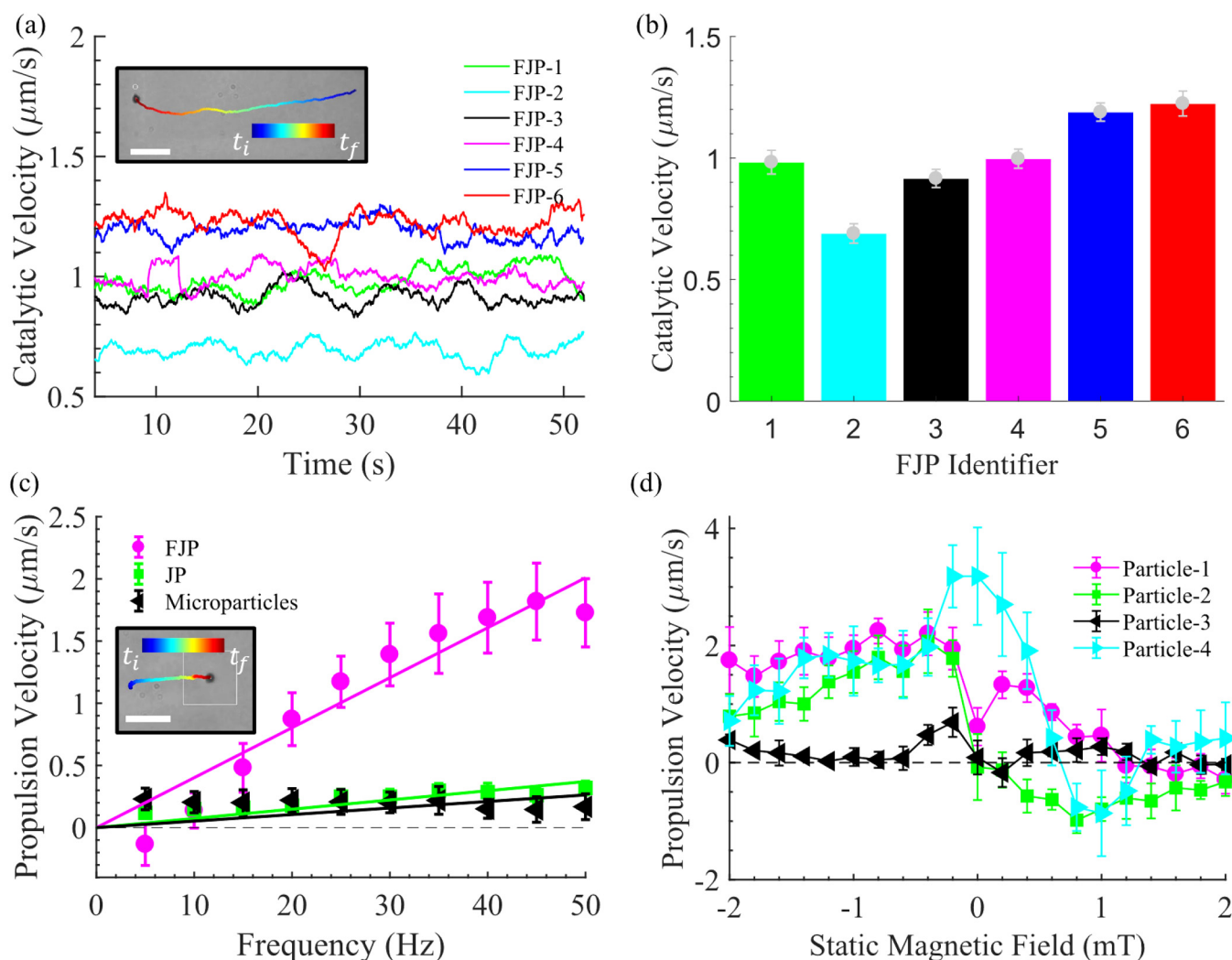
FIG. 2. Propulsion characterization of flagellated Janus particles. (a) The moving averaged velocity for an FJP undergoing catalytic propulsion within a 5% H_2O_2 solution (the window size of moving average was 30 points). The inset of (a) shows an FJP propelling under catalytic propulsion for 178 s; the scale bar is 10 μm. The total magnetic field applied was 3.11 mT. (b) Velocities from six different FJPs [the same ones examined in (a)], from at least three trials, with each being 30 s long under catalytic propulsion. The error bars show the standard deviation between the average velocity calculated over each of the three trials. (c) Velocity vs frequency curve for FJPs (magenta), un-flagellated Janus particles (JP, green), and microparticles (black) that were actuated using rotational magnetic fields; the solid line represents a linear fit to the velocity data points, and the dashed line represents the x-intercept. Six FJPs, ten Janus particles, and seven microparticles were examined, each with at least three independent trials each. The coefficients of determination (r-squared) were 0.92, 0.33, and −14.52 for FJPs, JPs, and microparticles, respectively. The minimum magnetic field was 3.40 mT (at 5 Hz), and the maximum was 13.97 mT (at 50 Hz). The inset of (c) shows an FJP propelling under rotational magnetic field propulsion for 15 s; the scale bar is 10 μm. (d) FJPs were rotated between 40 and 45 Hz under different static magnetic fields. As the static magnetic field is altered, the propulsion velocity of each FJP is affected differently, with some being able to switch propulsion directions and others experiencing reduced velocities. Four FJPs were examined, each with at least three independent trials each. The maximum and minimum magnetic fields applied were 12.26 mT (at 0 mT static field) and 12.65 mT (at −2 or 2 mT static field).

TABLE I. Average velocity and standard deviation under catalytic propulsion.

FJP	1	2	3	4	5	6
μ (μm/s)	0.98	0.69	0.92	1.00	1.19	1.22
σ(μm/s)	0.049	0.04	0.037	0.039	0.037	0.051

(x axis) was analyzed during these experiments; hereafter, this is referred to as propulsion velocity. The tangential velocity was found to be significantly smaller in magnitude, constant between experiments, and had no correlation with frequency; we attribute this to small thermal fluctuations or slight internal flows in the sample chamber. As was discussed in the previous work, the coil

forms of the attached flagella remained normal[42] in these salt concentrations and did not change form as shear rates increased.[37] The random distribution of flagella along the hemisphere of the FJPs caused microswimmers to swim either along or against the heading vector [Fig. 1(c)] and was corrected in a post-processing data analysis such that all FJPs had swimming velocities with the same sign along the rotation axis. The averaged velocity results between six different FJPs, each with at least three trials each, are shown in Fig. 2(c), and the solid magenta line represents a linear fit of the data. To confirm that propulsion was being caused solely by the attached flagella, control experiments involving magnetic microparticles and un-flagellated Janus particles of $4\,\mu$m diameter were performed. The magnetic microparticles did not exhibit any correlation with frequency but did experience a small and near constant velocity, which we can attribute to slight internal flow; this is in good agreement with literature predicated symmetry limitations that a symmetric microparticle cannot propel under rotation in a Newtonian fluid.[15,36] Examining un-flagellated Janus particles did reveal that some Janus particles could propel even without flagellar surface coating being present, but these were rare occurrences; the most likely explanation for this is that during the fabrication process (see Materials and Methods), small non-uniform platinum geometric irregularities fixed themselves onto the microparticle surfaces, thereby explicitly breaking symmetry. While this does result in a weak correlation with frequency, the application of flagellar functionalization guaranteed the propulsion of FJPs under rotating magnetic fields by having a stronger correlation with frequency during the same experiments. The extra source of geometric irregularity increased the probability of propulsion among individual flagellated Janus particles.

Swimming behavior was achievable for all FJPs examined, with their overall velocity profile being mostly linear with frequency; however, there was a small performance decrease observed after 45 Hz, possibly because of a step-out frequency. Due to the offset of the flagellar hemisphere from the magnetic dipoles, which is randomly caused during the fabrication process [see Materials and Methods; see Fig. 1(a)], the velocity of FJPs under swimming propulsion could be modulated by changing the magnitude of the applied static field. To demonstrate this, the superimposed static field was iterated between -2 and $2\,$mT in $0.2\,$mT increments, while the FJP was rotated constantly at 40 or 45 Hz. The static field altered the pitch of the FJP dipoles about the heading vector [Fig. 5(b)] and induced a small secondary rotation about the axis of the dipoles. As seen in Fig. 2(d), the velocity behavior of FJPs rotating at a constant frequency changed significantly under different static fields. In some cases, the FJPs reversed the swimming direction or achieved optimal propulsion at different static fields. These velocity vs static field curves varied considerably between individual FJPs and can potentially be used as a parameter in the future to allow for optimization of individual propulsion velocities or could potentially allow for non-homogeneous behavior within swarms of FJPs when actuated under the same globally applied rotating magnetic field input.

Mean square displacement analysis

A two-dimensional mean square displacement (MSD) analysis was performed to compare both catalytic and swimming propulsion modes of FJPs. The two-dimensional mean square displacement was calculated using

$$\langle r_\tau^2 \rangle = \frac{1}{N-\tau} \sum_{i=1}^{N-\tau} (r(t_i + \tau) - r(t_i))^2, \tag{2}$$

where $\langle r_\tau^2 \rangle$ is the scalar MSD at a specific lag time τ, N is the number of time steps for a given trajectory, r is the position vector, and t_i is the ith time increment.[43] An MSD profile is created when MSD is calculated for a range of lag times and ensemble averaged over several trials. For both the rotating and catalytic propulsion cases, the MSD profiles were modeled using

$$\langle r_\tau^2 \rangle \propto 4D\tau^\alpha, \tag{3}$$

where D is generalized diffusion and α is the anomalous diffusion exponent; this model was selected to understand how both motion modes diffused through the fluid and compare them with a particle undergoing Brownian motion. Both terms D and α were fitted from positional data collected from FJPs under both swimming and catalytic propulsion, using a delayed rejection adaptive Metropolis (DRAM) Markov Monte Carlo technique.[44] The smallest lag time was 1/30th of a second, and N was at least 300 for both propulsion modes during experiments. Fittings for both propulsion modes were obtained with a range of lag times between 1 and 5 s using the DRAM technique, where no prior distributions were set for either D or α, and a chain length of 100 000 iterations was utilized; the average of the last 10% of the chain was used to estimate the two parameters for each propulsion mode. The results of the MSD analysis can be seen graphically in Fig. 3, which compares the results from swimming (45 Hz) and catalytic propulsion. Three FJPs were examined under rotation, six were examined under catalytic propulsion [the same ones used in Figs. 1(a) and 1(b)], and seven ferromagnetic microparticles ($4\,\mu$m diameter) were examined under pure Brownian motion conditions with no applied magnetic fields to compare as a control; all particles examined had at least three independent trials each.

The estimated generalized diffusion coefficient for the swimming propulsion was $0.24\left(\frac{\mu m^2}{s^\alpha}\right)$, and the anomalous diffusion exponent was 1.92. The estimated generalized diffusion coefficient for the catalytic propulsion was $0.06\left(\frac{\mu m^2}{s^\alpha}\right)$, and the anomalous diffusion exponent was 1.93. The estimated generalized diffusion coefficient for the zero-propulsion scenario for microparticles was $0.02\left(\frac{\mu m^2}{s^\alpha}\right)$, and the anomalous diffusion exponent was 0.85; this slight subdiffusive behavior occurred from post-processing used to account for slight tracking errors and drift.[45] Both motion modes had comparatively similar anomalous diffusion exponents, but there was almost an order of magnitude difference between generalized diffusion coefficients of swimming and catalytic propulsion, respectively. The MSD for the catalytic propulsion was consistent at both short and large lag times, while the swimming propulsion displayed a flat MSD at short lag times and a more uniform profile as lag time increased. The flat MSD profile at short lag times was the result of the initial transient rotation of the FJPs as they started
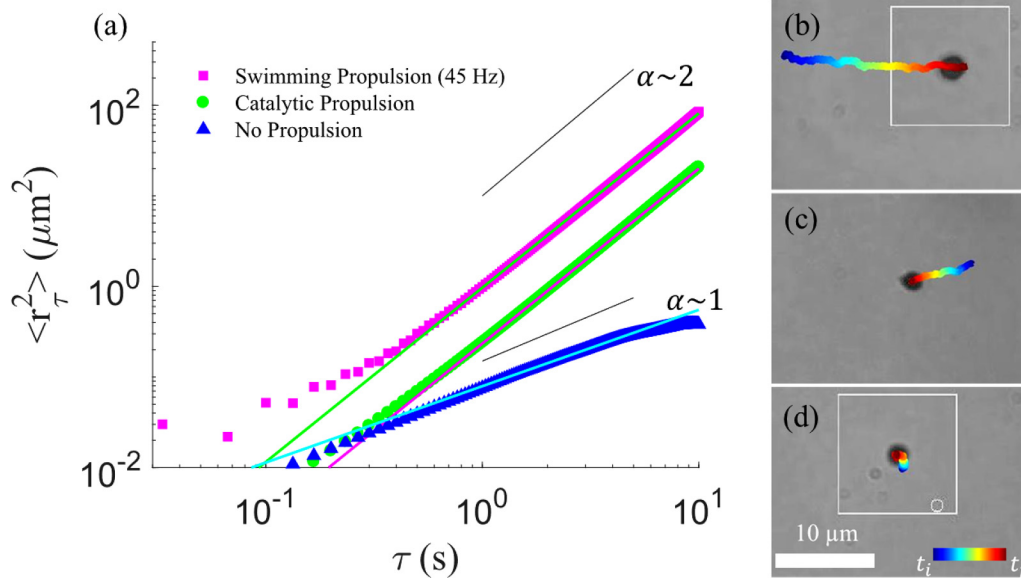
FIG. 3. Mean square displacement analysis. (a) Mean square displacement for a flagellated Janus particle under both rotating and catalytic propulsion. Contrasting colored solid lines represent fittings to Eq. (3) for swimming propulsion (FJPs, raw data: magenta, fit: green), catalytic propulsion (FJPs, raw data: green, fit: magenta), and no propulsion (microparticles, raw data: blue, fit: cyan), respectively. Total magnetic fields for swimming propulsion, catalytic propulsion, and Brownian conditions were 12.65, 3.11, and 0 mT, respectively. Three FJPs were examined under rotation, six FJPs were examined under catalytic propulsion, and seven microparticles were examined under Brownian conditions (no rotation, no catalysis). (b) and (c) Show the trajectories for FJPs propelling under swimming and catalytic propulsion, while (d) shows the trajectory for a particle under Brownian conditions. Each trajectory in (b) and (c) shows 20 s of observation.

from rest at the beginning of the experiment; this transient behavior disappears after a lag time of 1 s. Despite these differences, both motion modes displayed ballistic behavior since their anomalous diffusion coefficients were greater than 1 and is consistent with the results presented in the previous sections.

Trajectories under feedback control

FJPs were next examined to determine whether or not consistent directional control was possible using both propulsion modes. For this experiment, only the heading angle θ was of interest, with other parameters kept constant. The heading angle θ was manipulated using the simple proportional controller,

$$\dot{\theta} = k\alpha, \quad (4)$$

$$\alpha = \phi - \theta, \quad (5)$$

with $\dot{\theta}$ being the time derivative of θ, k is the user specified gain, ϕ is the desired heading angle relative from the FJP's current position (x_c, y_c) to the target position (x_t, y_t), and α is the angular difference between the desired heading angle ϕ and the actual heading angle of the particle θ. The target location was user specified as a coordinate within the field of view, while the FJPs current position was estimated using its centroid. The initial heading angle is arbitrarily selected before the experiments, while the desired heading angle is calculated as $\phi = \arctan\frac{y_t - y_c}{x_t - x_c}$. The equations for this proportional

controller are transferable between both motion modes as described by Eqs. (6)–(9) in Materials and Methods. The gain, k, was chosen to be 5 throughout the experiments to ensure that θ achieved steady state quickly; this was determined through experimental trial and error. The results of four FJPs can be seen in Fig. 4, with (a) and (b) showing the trajectories under rotational magnetic fields (50 Hz and 2 mT, 19 Hz and 0.2 mT and $B_r = 0.5f$, respectively) and (c) and (d) showing trajectories under catalytic propulsion with two different offset angles (∼45° and ∼0°) directed by a 2 mT static field; the magenta points and dashed lines represent the target destinations and shortest paths, respectively. After the displacement error between the propelling FJPs' centroid and the target point (magenta point) became small, the target point was manually iterated to the next location in the sequence and the FJP would attempt to reach it. FJPs under swimming propulsion were found to easily follow the intended trajectories repeatably and quickly. FJPs under catalytic propulsion were also highly consistent but were prone to experiencing a significant variation due to their heterogeneous propulsion offset angles Ψ. An example of this can be seen in Fig. 4(c), where the FJP, with a Ψ of ∼45°, performed exaggerated parabolic trajectories as it proceeded to each target destination. An FJP with a small Ψ (∼0°), as seen in Fig. 4(d), could perform the intended trajectory equivalently to the FJPs actuated under rotating magnetic fields [Figs. 4(a) and 4(b)]. The FJPs under swimming propulsion in Figs. 4(a) and 4(b) took 42 s (50 Hz) and 95 s (19 Hz), respectively, while under catalytic propulsion in (c) and (d), the trajectories took 287 and 316 s, respectively.
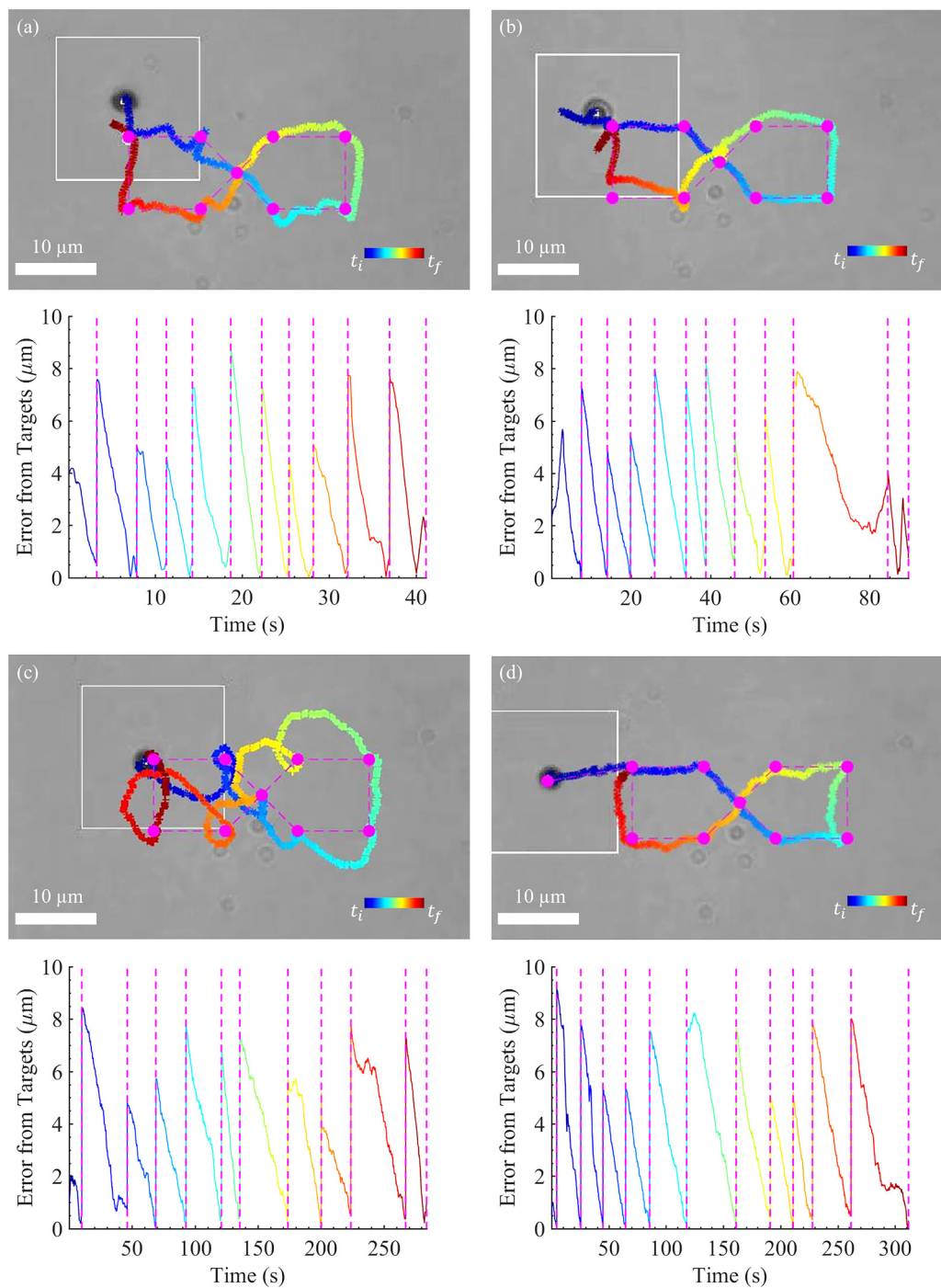
FIG. 4. Feedback control and performance of flagellated Janus particles. (a)–(d) Selected trajectory of a FJP under feedback control using (a) and (b) rotating magnetic fields and (c) and (d) chemical catalyzation. Magenta colored dots represent the desired destination points of the FJP, while the dashed magenta line represents the most direct path between points. Included with (a)–(d) are the error curves with magenta dashed lines separating the target points. The rotation frequency and the static magnetic field for (a) was 50 Hz and 2 mT; $B_r = 0.175f$ with a total magnetic field of 13.97 mT. The rotation frequency and the static magnetic field for (b) was 19 Hz and 0.2 mT; $B_r = 0.5f$ with a total magnetic field of 15.11 mT. The offset angles for (c) and (d) were $\sim 45°$ and $\sim 0°$, respectively; both experiments had a total magnetic field of 3.11 mT. The window size for the moving averaged velocity was 100 points for all trajectories.

Using the trajectories from Figs. 4(a)–4(d), the error was quantitatively measured as a distance from the intended target magenta points, and the actual trajectory performed by the FJPs is displayed as a color bar. In all four scenarios, the error between the FJPs and each respective target location always decayed to near zero except for one case in Fig. 4(b) where it could not reach one of the target locations. It is important to reiterate that, despite the missed target point in the trajectory of Fig. 4(b), the FJP still reasonably came within a small error of the other target points within a reasonable time. Consistent with the previous work, the FJP with

a $\Psi \cong 45°$ could still reach all of the target locations, although having largely curved trajectories [Fig. 4(c)]. However, if an FJP was ever encountered that had a $\Psi > 90°$, the target points would never be reached, as was demonstrated in the previous work.[40]

Propulsion in a nonlinear fluid

Flagellated Janus particles were deployed inside a 1% poly (ethylene oxide) solution (PEO, Sigma Aldrich, 189464-250G) to understand their behavior within a known nonlinear fluid. Unlike
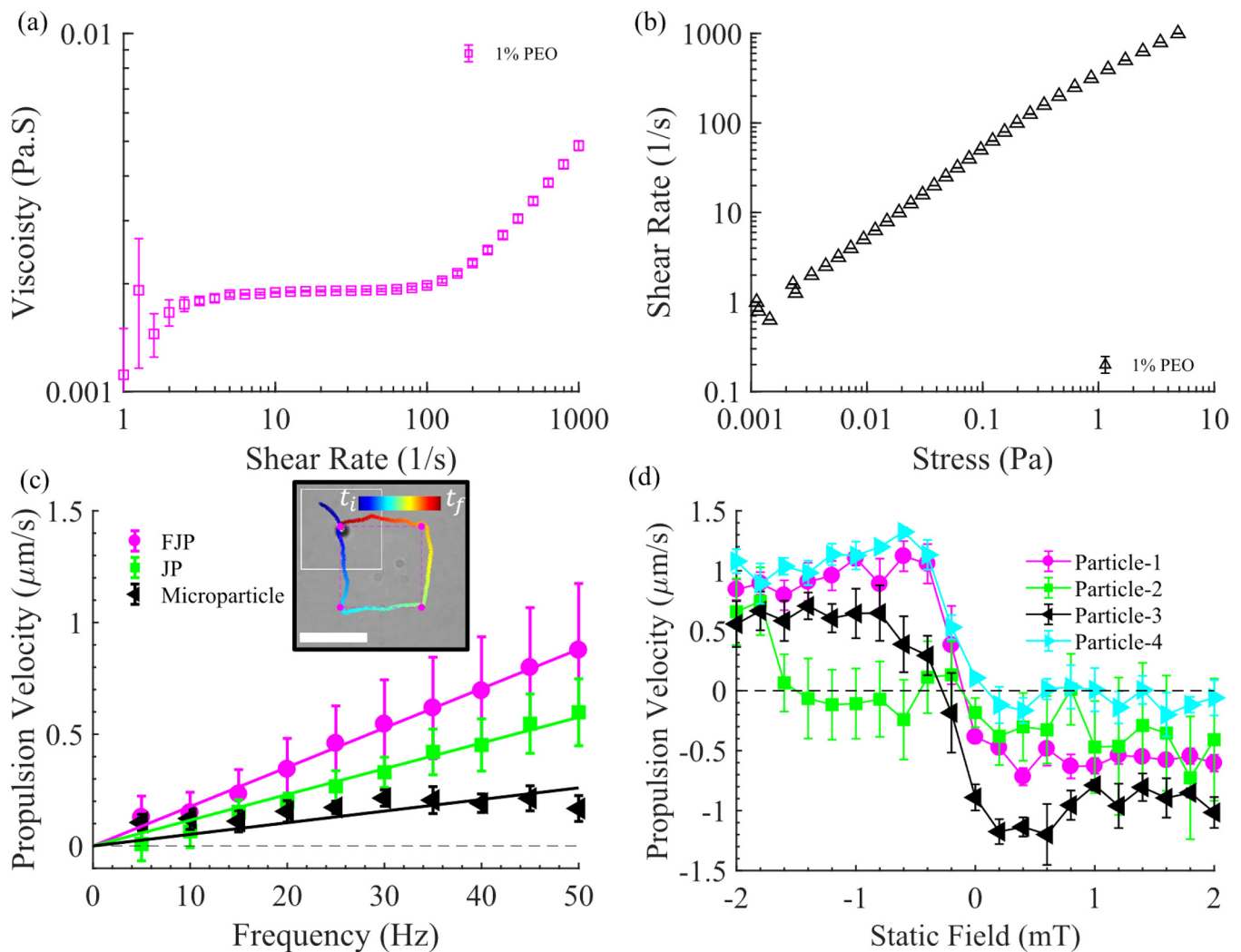
FIG. 5. Propulsion in Poly (ethylene oxide) (PEO). (a) Viscosity vs shear rate curve and (b) the shear rate vs stress curve for 1% PEO. Three independent rheology tests were performed for PEO and then averaged together. (c) Velocity vs frequency curve for FJPs, JPs, and microparticles actuated in 1% PEO. The *r*-squared values were 0.99, 0.98, and −0.92 for FJPs, JPs, and microparticles, respectively. Five FJPs, seven Janus particles, and seven microparticles were examined, with at least three independent trials each. The minimum magnetic field was 3.40 mT (at 5 Hz), and the maximum was 13.97 mT (at 50 Hz). The inset of (c) shows an FJP propelling in 1% PEO under rotating magnetic fields for 54 s; the scale bar is 10 μm. (d) Propulsion velocity vs static field for FJPs rotated at 45 Hz. The maximum and minimum magnetic fields applied were 12.26 mT (at 0 mT static field) and 12.65 mT (at −2 or 2 mT static field).

the Newtonian fluids used previously (saline solution, de-ionized water), non-Newtonian fluids have viscosities that are shear rate dependent. Using a Discovery Hybrid Rheometer (DHR-3, TA Instruments), a shear sweep was performed using a 40 mm 4° cone-plate geometry under an incremental shear rate of 1–1000 (1/s) over three independent trials. The rheology characterization of 1% PEO is shown in Figs. 5(a) and 5(b) where both the viscosity vs shear rate and the shear rate vs stress are shown, respectively. Interestingly, the viscosity vs shear rate curve [Fig. 5(a)] indicates that a shear-thickening effect occurs after a shear rate of 100 (1/s) and with the stable shear rate vs stress curve [Fig. 5(b)], indicating that this behavior is genuine and not the result of fluid being ejected from the geometry under the high shear rates. The literature suggests that 1% PEO should be a shear thinning fluid; however, their reported molecular weights were several magnitudes higher than the 100 000 molecular weight of the PEO used in these experiments;[46] making the estimated shear-thickening behavior a reasonable possibility. The FJPs discussed previously could achieve shear rates between 31.4 and 312 (1/s) under respective rotational magnetic field frequencies between 5 and 50 Hz, well within the range of the observed non-linear behavior of the fluid.

FJPs were deployed within the 1% PEO solution (with no H_2O_2) and made to replicate the experiments shown previously in Figs. 2(c) and 2(d) to understand how frequency and static magnetic field iteration effected their velocity profiles. The results of these swimming experiments can be seen in Figs. 5(c) and 5(d) where there is a strong linear relationship trend present in FJPs actuated in 1% PEO; however, the overall velocity of the FJPs was reduced [in comparison with Fig. 2(c)] from 2 to 0.87 μm/s at 50 Hz. While examining control experiments for bare microparticles (4 μm diameter, no flagella) suspended in 1% PEO, it was observed that there was no propulsion velocity relationship with frequency, with the near constant residual velocities at each frequency being the result of Brownian motion; this rules out that any spontaneous symmetry breaking effects are occurring in the fluid.[35] However, when examining the propulsive behavior of Janus particles under a rotating magnetic field, without attached flagellar, there was a strong correlation between velocity and frequency. This correlation is highly unexpected, especially considering there was only a weak correlation with frequency present in the Newtonian saline solution. One possible explanation is that the small propulsive effects from geometric surface deformities on the Janus particles may have been amplified by the nonlinear behavior of 1% PEO, as propulsion was ubiquitous between nearly all Janus particles examined. Catalytic propulsion was not observed in 1% PEO that contained a 5% concentration of H_2O_2; the increased viscosity was most likely too large for the propulsion mechanism to overcome. This demonstrates, however, that the swimming propulsion can be situationally more useful depending on the working fluid.

When examining the static field variation [Fig. 5(d)] for FJPs rotated at a constant frequency (45 Hz), it is clear that FJPs maintain similar relationships with a static field variation that were expressed previously in Fig. 2(d) but again with a reduced velocity overall, and clear heterogeneities in the curves are most likely the result of differences in the flagella spatial distribution for each respective particle. From these results, we can conclude that not only are these FJPs useful in Newtonian fluids but can also achieve reasonable performance inside a shear-thickening regime of a non-Newtonian fluid; surprisingly, Janus particles with surface deformities can propel in 1% PEO without the need for flagellar surface coatings.

CONCLUSIONS

Flagellated Janus particles (FJPs) were fabricated to have hemispheres consisting of platinum and bacterial flagella, allowing them to be actuated using either catalytic or swimming propulsion. These are the first Janus particles that could be actuated using both catalytic and flagella-based swimming propulsion modes interchangeably. Bacterial flagella distributed along one of the FJP hemispheres allowed for a non-time reversible swimming locomotion to occur when rotated by a magnetic field. When exposed to an H_2O_2 solution, the platinum coating on the other hemisphere of the FJPs acted as a catalyst and initiated catalytic propulsion; however, the catalytic propulsion only achieved velocities of a few microns per second under current experimental settings. This will be improved in the future by adjusting the platinum surface coatings and diameter of the Janus particles. It was demonstrated that velocities of FJPs were mostly linear with the rotation frequency, while their velocities under catalytic propulsion were nearly constant with time for all FJPs examined. Control experiments in Newtonian fluids revealed that bare microparticles had no correlation with the frequency, while Janus particles (without flagella) only had a weak correlation with the frequency, most likely the result of surface deformities during fabrication. Under swimming locomotion, a superimposed static magnetic field could be used to adjust the velocity and direction of an FJP rotating at a constant frequency. A mean square displacement analysis was performed to show that both motion modes displayed ballistic behavior at short time scales, with the generalized diffusivity of the swimming propulsion being an order of magnitude higher than the catalytic propulsion during experiments. Using proportional feedback control, FJPs could be made to perform pre-selected trajectories under both motion modes. However, the offset angle of the propulsion vector to the applied static magnetic field could produce exaggerated trajectories for catalytically propelling FJPs. FJPs were suspended inside a non-Newtonian poly (ethylene oxide) solution (PEO) that was measured to have shear-thickening properties at the actuation frequencies of the FJPs. Catalytic propulsion was not achievable in 1% PEO with a 5% H_2O_2 concentration; however, FJPs were able to propel in 1% PEO using swimming propulsion while retaining a linear velocity profile and exhibiting similar propulsive dependencies on static fields such as the Newtonian solutions. While bare microparticles under the same control experiments did not display any velocity relationship with frequency and did not experience any spontaneous symmetry breaking propulsion,[35] the un-flagellated Janus particles, however, did display a high correlation between the velocity and frequency. Our theory is that the slight surface deformities present on the Janus particles, combined with the nonlinear behavior of the poly (ethylene oxide) solution, are enough to allow free propulsion in PEO using rotating magnetic fields. Thus, in this particular nonlinear fluid, flagellar surface coating on Janus particles may not be necessary.

While not fully explored here, flagella are polymorphically transformable under different fluidic conditions and can allow for different swimming behavior;[30] these differences in performance will be examined in future works for both motion modes. While the flagella used here are from living bacteria, their use inside the body can be facilitated through immune repression or by genetic engineering to remove the pathogen markers that trigger immune responses. FJPs could eventually be used as an *in vivo* diagnostic tools where fluidic properties are directly related to the conformation of the FJP flagellar coating. Equipping other surface coatings, such as gold or silver instead of platinum, will allow for thermal propulsion when exposed to laser excitation and could potentially be used for applications such as hyperthermia. Optimizing the flagella distribution along the avidin coated hemisphere will also be investigated. Finally, closed-loop 3D control will be explored in future works to expand the capabilities of FJPs for *in vivo* navigation and sensing.

MATERIALS AND METHODS

Coil system

A triaxial approximate Helmholtz coil system was utilized to generate static and rotating magnetic fields in 3D for all experiments. The swimming locomotion of an FJP relied on rotating and static magnetic fields governed by

$$\overrightarrow{B_1} = \begin{bmatrix} -B_s \cos\theta + B_r \sin\theta \cos\omega t \\ B_s \sin\theta + B_r \cos\theta \cos\omega t \\ B_r \sin\omega t \end{bmatrix}, \qquad (6)$$

$$\vec{n} = \begin{bmatrix} -\cos\theta & \sin\theta & 0 \end{bmatrix}, \qquad (7)$$

where $\overrightarrow{B_1}$ is the magnetic field vector, B_r is the amplitude of the rotating magnetic field, B_s is the amplitude of the static magnetic field, ω is the rotational frequency of the field, θ is the heading angle in the x–y plane, t is time, and $\vec{n}$ is the direction vector. Dipoles of the FJPs align with $\overrightarrow{B_1}$ as it rotates in the plane perpendicular to the direction vector $\vec{n}$ and can rotate either clockwise or counterclockwise about the direction vector when viewed from behind. Propulsion along $\vec{n}$ indicates that swimming is occurring because of the surface coated flagella. As seen in Figs. 2(c) and 2(d), the velocity of the FJP can be directly modulated by changing either the frequency or the superimposed static magnetic field. To ensure that the dipoles remained in synchronization with the magnetic field, the amplitude of the rotating magnetic field was scaled with increasing frequency f. This scaling was selected to be either $B_r = 0.175f$ (50 Hz max) or $B_r = 0.5f$ (19 Hz max) depending on what frequency range or magnetic field values are needed for the particular experiment. The maximum and minimum total magnetic fields shown in figure captions for rotation experiments were calculated using Eq. (6); this resulting vector was multiplied by an amplification factor of 1.55 to account for the "approximate" nature of the Helmholtz coils and then the norm of the vector was calculated to provide the total magnetic field. A lower scaling allowed for frequencies as high as 50 Hz, while the higher scaling allowed for larger magnetic fields but limited frequency to ≤20 Hz.

When an FJP was undergoing chemical propulsion, the velocity profile of the FJP could not be controlled directly using external stimuli; however, the heading direction of the FJP under catalytic propulsion could be controlled by static fields using a simplified version of Eq. (6) where $\omega = 0$,

$$\overrightarrow{B_2} = \begin{bmatrix} -B_S \cos(\theta) \\ B_s \sin(\theta) \\ B_z \end{bmatrix}, \qquad (8)$$

$$\vec{p} = \begin{bmatrix} \cos(\theta - \Psi) & \sin(\theta - \Psi) & 0 \end{bmatrix}. \qquad (9)$$

The propulsion vector $\vec{p}$ under catalytic propulsion usually offsets the magnetic field vector $\overrightarrow{B_2}$ by an offset angle Ψ, which is randomized during the fabrication process. For all experiments involving closed-loop control, Ψ was assumed to be zero, and future works will involve estimating and optimizing Ψ for more accurate control in real time. The maximum and minimum total magnetic fields shown in figure captions for catalytic experiments were calculated using Eq. (8); this resulting vector was multiplied by an amplification factor of 1.55 to account for the "approximate" nature of the Helmholtz coils and then the norm of the vector was calculated to provide the total magnetic field. Figures 1(c) and 1(d) show schematics of both swimming and catalytic propulsion modes for Eqs. (6) and (7) and Eqs. (8) and (9), respectively.

The Helmholtz coil system was mounted on the top of a Leica DM IRB inverted microscope (type 090–132.701), and a 63× objective was used to visualize the FJPs. A complementary metal oxide semiconductor (CMOS) camera (Point Grey, FL3-U3-13Y3M-C) recording at 30 frames per second (fps) was used to record experiments in real time. Programmable power supplies (KEPCO-BOP-5M) were linked to a data acquisition board (National Instruments, DAQ) and interfaced with a customized LabVIEW, which could adjust the desired magnetic field parameters. The LabVIEW program could track the centroids of observed particles using image binarization and morphological filters. Post-processing was carried using MATLAB where positional data of the FJPs were converted to velocity data by taking the positional changes of FJPs between individual camera frames. The pixel distance was found to be $0.152\,\mu m$/pixel, with the camera resolution being 512×640.

Fabrication of flagellated Janus particles

Streptavidin coated ferromagnetic microparticles ($10.6\,\mu m$, Spherotech, IL) at 0.5% (w/w) concentration within a de-ionized water solution were distributed as a monolayer on a glass substrate. The surface of the glass substrate was made hydrophilic using UV-Ozone such that the aqueous solution spreads out evenly along the surface. The prepared sample was then heated up to 80 °C on a hot plate to evaporate the water, leaving only the microparticle monolayer on the substrate. Reactive ion etching (RIE) was utilized to separate the clustered microparticles from each other by etching the bead surface uniformly. To ensure the self-propulsion with the catalytic reaction of H_2O_2, a platinum (Pt) layer with a thickness of 20 nm was coated on the top half of the microparticles using an e-beam thermal evaporator (Temescal CV-8 e-beam evaporator).

Platinum was evaporated at a slow rate of 0.02 nm/s to ensure high-quality deposition. The coated microparticles were then detached from the glass surface by gently washing the substrate with de-ionized water and agitated with a paint brush. The final size of the Janus particles was measured to be ~4 μm. Streptavidin coated ferromagnetic microparticles (4 μm, Spherotech, IL) were used for control experiments. This process is also outlined in the previous work, where scanning electron microscopy images were used to confirm the presence of the platinum surface coating.[40]

An avidin coating along the uncoated hemisphere of the Janus particles remained intact after the fabrication process. While the size of this area along the hemisphere is variable, it can still be utilized to chemically attach single-end biotinylated flagella filaments along the surface of the Janus particle. The flagella were isolated from *S. typhimurium* (SJW 1103) and repolymerized using methods adapted from Asakusa's original procedures[47,48] and established in the previous work.[30,31,37] We used *S. typhimurium* simply because we have the most experience with it, but other bacteria such as *E. coli* can also be used to harvest flagella.[49] Non-pathogenic *S. typhimurium* (SJW 1103) was cultured in 10 l of Luria-Bertani (LB) broth, with additional additives in percent by weight including: 1.00% yeast extract, 1.00% tryptone, 0.30% glucose, 0.66% dipotassium phosphate, and 0.03% monopotassium phosphate. After a 12–16 h incubation-shaking process (36 °C, 130 rpm), the culture media were placed inside 50 ml centrifuge tubes and centrifuged with a 3500 relative centrifugal force (rcf) for 35 min, causing the bacteria in the LB broth to become pelleted to the bottom of the centrifuge tubes; the supernatant was then removed and discarded into a liquid biohazard container. Centrifuge tubes with pelleted bacteria had more bacteria culture solution added, and the centrifugation process was repeated until all the remaining solution was exhausted. The pelleted bacteria were then resuspended into a 0.01 M potassium phosphate buffer (pH 6.5, referred to as polymerization buffer) with a 150 mM of NaCl using a piston pipette; the bacteria suspension was concentrated together into a single tube with a final volume of 50 ml. This concentrated solution of bacteria was then vortexed for more than 20 min to mechanically shear the flagella from the bacterial bodies[37] and subsequently centrifuged for 15 min at 16 000 rcf in order to pellet bacterial bodies while keeping the flagella in suspension; the supernatant was transferred then to new tubes, while the bacterial pellets were disposed off into a biohazard box. The flagellar solution was then centrifuged at 100 000 rcf for 1 h to pellet the flagella. The purified flagellar pellet was then resuspended in polymerization buffer with a final volume of 1.5 ml per pellet; further purifications at 100 000 rcf for 1 h were performed as needed depending on the researcher's judgment. Roughly 20% of the isolated flagella by volume were taken and mixed with EZ-Link™ NHS-Biotin (Thermo Fisher Scientific, 20217) using the standardized process outlined by Thermo Fisher. After 30 min, the biotin complex was completely bound to the surfaces of the flagella. The biotinylated flagella solution was then centrifuged at 16 000 rcf for 15 min to remove any excess biotin while leaving the flagella in suspension. Both the biotinylated and nonbiotinylated flagellar solutions were then placed in a water bath at 65 °C for 10 min in order to thermally depolymerize the flagella into constituent flagellin monomers. Both solutions were then centrifuged at 150 000 rcf for

1 h to remove any excess proteins, debris, or remaining excess biotin, while flagellin monomers remained in suspension. The supernatants containing flagellin monomers were then transferred to new centrifuge tubes. The biotinylated monomers were then introduced into a 2 M sodium phosphate solution of an equal volume (750 μl each) and incubated for 30 min at 36 °C in order to turn the monomers into short flagella (referred to as seeding particles). The seeds were then introduced into the non-biotinylated monomers in a 1:5 ratio and uniformly mixed by vortexing for 5 min; the mixture was left to incubate for 48 h at room temperature. The resulting repolymerized flagella were between 10 and 25 μm in length and had biotin surface coating at one of their end points.[37] The repolymerized flagella were usually so highly concentrated that they looked like a white gelatinous mass. The repolymerized flagella (gelatinous mass) were then gently suspended using a 0.01 M potassium phosphate (pH 7.5, conjugation buffer) with 150 mM of NaCl solution, centrifuged at 10 000 rcf for 1 h and resuspended using a 0.01 M potassium phosphate (pH 7.5, referred to as conjugation buffer) with 150 mM of NaCl solution for a total volume of 1.5 ml. A Cy3 dye (Sigma Aldrich, GEPA23001) was reconstituted in conjugation buffer (1.5 ml) and then mixed in a 1:1 ratio with the flagellar solution; 1 M of sodium bicarbonate was added (5% of the final volume) to help the dye attach to the flagella. After 2 h, the Cy3 labeled flagella were centrifuged at 100 000 rcf, pelleted, and resuspended using the conjugation buffer for a total volume of 1.5 ml.[37] The final centrifugation and resuspension processes sheared the repolymerized flagella, reducing their overall length to roughly half.

Approximately 5–20 μl of flagellar solution was placed in a 5 ml centrifuge tube containing 1–2 μl of Janus particle solution; this mixture was gently shaken for 5 min to ensure flagellated Janus particle formation. Avidin–biotin bonding, between the microparticle and the flagellar ends, is the strongest non-covalent bond found in nature. Flagellated Janus particles were visualized using an Olympus confocal microscope (FV3000), and a z-stack was used to produce the image shown in Fig. 1(b). The distribution of flagella along the hemisphere was highly random, but it was visually estimated that anywhere from one to six flagella were present along the surfaces of the particles with average lengths of about 5 μm, with the longest flagella observed being about 8 μm; while not discussed in this paper, it was found in the previous work that velocity performance improves as flagella length increases.[31] After the fluid medium of interest is added to the flagellated Janus particle solution, bringing the total volume of the centrifuge tube to 750–1000 μl, a portion of the fluid is loaded into a polydimethylsiloxane (PDMS) chamber 3 mm in diameter and 1 mm in height situated on a No. 1.5 glass cover slide (25 × 30 mm²). The chamber was then sealed using a smaller No. 1.5 glass cover slide (18 × 18 mm²) and placed in the center of the approximate Helmholtz coil system where it was ready for experimentation.

SUPPLEMENTARY MATERIAL

See the supplementary material for a video demonstrating select experiments performed by flagellated Janus particles.

AUTHORS' CONTRIBUTIONS

L.W.R. performed all experiments and analysis presented within this paper. J.T. performed all flagella isolation and labeling processes. X.Z. fabricated the Janus particles used throughout experiments. M.O. assisted with experiments and analysis. M.J.K. was the principal investigator and provided all resources necessary to carry out these experiments.

DATA AVAILABILITY

The data that support the findings of this study are available from the corresponding author upon reasonable request.

REFERENCES

[1]S. Campuzano *et al.*, "Magnetic Janus particles for static and dynamic (bio) sensing," Magnetochemistry **5**, 47 (2019).

[2]A. Kirillova, C. Marschelke, and A. Synytska, "Hybrid Janus particles: Challenges and opportunities for the design of active functional interfaces and surfaces," ACS Appl. Mater. Interfaces **11**, 9643–9671 (2019).

[3]A. Kirillova *et al.*, "Hybrid hairy Janus particles decorated with metallic nanoparticles for catalytic applications," ACS Appl. Mater. Interfaces **7**, 21218–21225 (2015).

[4]L. Baraban *et al.*, "Catalytic Janus motors on microfluidic chip: Deterministic motion for targeted cargo delivery," ACS Nano **6**, 3383–3389 (2012).

[5]L. Baraban *et al.*, "Transport of cargo by catalytic Janus micro-motors," Soft Matter **8**, 48–52 (2012).

[6]Y. Yi, L. Sanchez, Y. Gao, K. Lee, and Y. Yu, "Interrogating cellular functions with designer Janus particles," Chem. Mater. **29**, 1448–1460 (2017).

[7]Z. Wu *et al.*, "A microrobotic system guided by photoacoustic computed tomography for targeted navigation in intestines *in vivo*," Sci. Robot. **4**, eaax0613 (2019).

[8]W. Uspal, "Theory of light-activated catalytic Janus particles," J. Chem. Phys. **150**, 114903 (2019).

[9]Z. Huang *et al.*, "Bacteria-activated Janus particles driven by chemotaxis," ACS Nano **12**, 6725–6733 (2018).

[10]X. Ma and S. Sánchez, "Bio-catalytic mesoporous Janus nano-motors powered by catalase enzyme," Tetrahedron **73**, 4883–4886 (2017).

[11]B. E. Pinchasik, H. Möhwald, and A. G. Skirtach, "Mimicking bubble use in nature: Propulsion of Janus particles due to hydrophobic-hydrophilic interactions," Small **10**, 2670–2677 (2014).

[12]P. S. Schattling, M. A. Ramos-Docampo, V. Salgueiriño, and B. Städler, "Double-fueled Janus swimmers with magnetotactic behavior," ACS Nano **11**, 3973–3983 (2017).

[13]W. Gao, M. D'Agostino, V. Garcia-Gradilla, J. Orozco, and J. Wang, "Multi-fuel driven Janus micromotors," Small **9**, 467–471 (2013).

[14]A. Brown and W. Poon, "Ionic effects in self-propelled Pt-coated Janus swimmers," Soft Matter **10**, 4016–4027 (2014).

[15]E. M. Purcell, "Life at low Reynolds number," Am. J. Phys. **45**, 3–11 (1977).

[16]S. Das *et al.*, "Boundaries can steer active Janus spheres," Nat. Commun. **6**, 8999 (2015).

[17]A. I. Campbell, S. J. Ebbens, P. Illien, and R. Golestanian, "Experimental observation of flow fields around active Janus spheres," Nat. Commun. **10**, 3952 (2019).

[18]P. Chattopadhyay and J. Simmchen, *Interactions of Different Janus Particles with Passive Tracers* (Cambridge Open Engage, Cambridge, 2019).

[19]J. R. Gomez-Solano, A. Blokhuis, and C. Bechinger, "Dynamics of self-propelled Janus particles in viscoelastic fluids," Phys. Rev. Lett. **116**, 138301 (2016).

[20]S. Ebbens, M.-H. Tu, J. R. Howse, and R. Golestanian, "Size dependence of the propulsion velocity for catalytic Janus-sphere swimmers," Phys. Rev. E **85**, 020401 (2012).

[21]H. Ke, S. Ye, R. L. Carroll, and K. Showalter, "Motion analysis of self-propelled Pt–silica particles in hydrogen peroxide solutions," J. Phys. Chem. A **114**, 5462–5467 (2010).

[22]S. Michelin and E. Lauga, "Geometric tuning of self-propulsion for Janus catalytic particles," Sci. Rep. **7**, 42264 (2017).

[23]U. Choudhury, L. Soler, J. G. Gibbs, S. Sanchez, and P. Fischer, "Surface roughness-induced speed increase for active Janus micromotors," Chem. Commun. **51**, 8660–8663 (2015).

[24]B. Halliwell, M. V. Clement, J. Ramalingam, and L. H. Long, "Hydrogen peroxide. Ubiquitous in cell culture and *in vivo*?," IUBMB Life **50**, 251–257 (2000).

[25]C. Lynn Humberston, B. S. Dean, and E. P. Krenzelok, "Ingestion of 35% hydrogen peroxide," J. Toxicol., Clin. Toxicol. **28**, 95–100 (1990).

[26]S. Pritchett, D. Green, and P. Rossos, "Accidental ingestion of 35% hydrogen peroxide," Can. J. Gastroenterol. **21**, 423217 (2007).

[27]P. Chatterjee, E. M. Tang, P. Karande, and P. T. Underhill, "Propulsion of catalytic Janus spheres in viscosified Newtonian solutions," Phys. Rev. Fluids **3**, 014101 (2018).

[28]S. K. Lai, Y.-Y. Wang, D. Wirtz, and J. Hanes, "Micro- and macrorheology of mucus," Adv. Drug Deliv. Rev. **61**, 86–100 (2009).

[29]U. K. Cheang, K. Lee, A. A. Julius, and M. J. Kim, "Multiple-robot drug delivery strategy through coordinated teams of microswimmers," Appl. Phys. Lett. **105**, 083705 (2014).

[30]J. Ali *et al.*, "Bacteria-inspired nanorobots with flagellar polymorphic transformations and bundling," Sci. Rep. **7**, 4098 (2017).

[31]J. Tang, L. W. Rogowski, X. Zhang, and M. J. Kim, "Flagellar nanorobot with kinetic behavior investigation and 3D motion," Nanoscale **12**, 12154–12164 (2020).

[32]U. K. Cheang, D. Roy, J. H. Lee, and M. J. Kim, "Fabrication and magnetic control of bacteria-inspired robotic microswimmers," Appl. Phys. Lett. **97**, 213704 (2010).

[33]W. Gao *et al.*, "Bioinspired helical microswimmers based on vascular plants," Nano Lett. **14**, 305–310 (2014).

[34]X. Wang *et al.*, "3D printed enzymatically biodegradable soft helical microswimmers," Adv. Funct. Mater. **28**, 1804107 (2018).

[35]L. W. Rogowski *et al.*, "Symmetry breaking propulsion of magnetic microspheres in nonlinearly viscoelastic fluids," Nat. Commun. **12**, 1116 (2021).

[36]E. Lauga and T. R. Powers, "The hydrodynamics of swimming microorganisms," Rep. Prog. Phys. **72**, 096601 (2009).

[37]L. W. Rogowski, M. Oxner, J. Tang, and M. J. Kim, "Heterogeneously flagellated microswimmer behavior in viscous fluids," Biomicrofluidics **14**, 024112 (2020).

[38]M. M. Stanton, J. Simmchen, X. Ma, A. Miguel-López, and S. Sánchez, "Biohybrid Janus motors driven by *Escherichia coli*," Adv. Mater. Interfaces **3**, 1500505 (2016).

[39]H. Xu *et al.*, "Sperm-hybrid micromotor for targeted drug delivery," ACS Nano **12**, 327–337 (2018).

[40]L. W. Rogowski *et al.*, in *2019 International Conference on Robotics and Automation (ICRA), Montreal, Canada* (IEEE, 2019), pp. 1352–1357.

[41] U. K. Cheang, F. Meshkati, D. Kim, M. J. Kim, and H. C. Fu, "Minimal geometric requirements for micropropulsion via magnetic rotation," Phys. Rev. E **90**, 033007 (2014).

[42] N. C. Darnton and H. C. Berg, "Force-extension measurements on bacterial flagella: Triggering polymorphic transformations," Biophys. J. **92**, 2230–2236 (2007).

[43] X. Michalet, "Mean square displacement analysis of single-particle trajectories with localization error: Brownian motion in an isotropic medium," Phys. Rev. E **82**, 041914 (2010).

[44] H. Haario, M. Laine, A. Mira, and E. Saksman, "DRAM: Efficient adaptive MCMC," Stat. Comput. **16**, 339–354 (2006).

[45] J. W. Mellnik *et al.*, "Maximum likelihood estimation for single particle, passive microrheology data with drift," J. Rheol. **60**, 379–392 (2016).

[46] K. W. Ebagninin, A. Benchabane, and K. Bekkour, "Rheological characterization of poly (ethylene oxide) solutions of different molecular weights," J. Colloid Interface Sci. **336**, 360–367 (2009).

[47] S. Asakura, G. Eguchi, and T. Iino, "Reconstitution of bacterial flagella *in vitro*," J. Mol. Biol. **10**, 42–IN9 (1964).

[48] S. Asakura, G. Eguchi, and T. Iino, "Unidirectional growth of salmonella flagella *in vitro*," J. Mol. Biol. **35**, 227–236 (1968).

[49] M. DePamphilis and J. Adler, "Purification of intact flagella from *Escherichia coli* and *Bacillus subtilis*," J. Bacteriol. **105**, 376–383 (1971).